JEE Journal of Ecological Engineering

Journal of Ecological Engineering 2024, 25(8), 207–221
https://doi.org/10.12911/22998993/190116
ISSN 2299–8993, License CC-BY 4.0

Received: 2024.05.30
Accepted: 2024.06.20
Published: 2024.07.01

Removal of Levofloxacin by Copper Doped Bismuth Oxide Thin Films under UV Light Irradiation

Fatkhiyatus Sa'adah[1,4], Heri Sutanto[2,4*], Hadiyanto Hadiyanto[3], Juhana Jaafar[5], Iir Ilsatoham[2,4], Ilham Alkian[1,4]

[1] Doctoral Program of Environmental Science, School of Postgraduate, Diponegoro University, Semarang, 50275, Indonesia

[2] Department or Physics, Faculty of Science and Mathematics, Diponegoro University, Semarang, 50275, Indonesia

[3] Department of Chemical Engineering, Faculty of Engineering, Diponegoro University, Semarang, 50275, Indonesia

[4] Smart Material Research Center (SMARC), Diponegoro University, Semarang, 50275, Indonesia

[5] Advanced Membrane Technology Research Center (AMTEC), Faculty of Chemical and Energy Engineering, Universiti Teknologi Malaysia, 81310 UTM Johor Bahru, Malaysia

* Corresponding author's e-mail: herisutanto@live.undip.ac.id

ABSTRACT

Pharmaceutical wastewater, including antibiotics, is being increasingly detected in the environment as a form of micropollutant. Researchers have progressively concentrated on integrating the advanced oxidation process (AOPs) with photocatalysts such as bismuth oxide (Bi_2O_3) to degrade antibiotics. The study involved the effective synthesis of pure Bi_2O_3 and Copper doped Bi_2O_3 (CBO) thin films using the sol-gel process. These thin films were then coated using the spray coating technique, and studied for their ability to degrade levofloxacin (LFX). The characterization including UV-Vis and XRD were used to analysed the properties of all synthesized thin films. 3% CBO thin films have the good quality compared with other thin films with the lowest energy band gap is 2.54 eV and crystallite size are 28.1938 nm. The degradation efficiency of 3% CBO thin films using photocatalysis is 85.95%. The degradation kinetic rate value is 0.00637 min^{-1} for pseudo-first-order kinetics and 0.00676 min^{-1} for pseudo-second-order kinetics. The reusability of CBO thin films was also evaluated to determine the sustainability of the thin films.

Keywords: thin films, antibiotic degradation, photocatalysis, bismuth oxide.

INTRODUCTION

Nowadays, water pollution has become a major issue for many researchers, due to a variety of contaminants such as pesticides, herbicides, dyes, and pharmaceuticals [1]. Pharmaceutical usage has expanded the diversity of contaminants in the environment, resulting in an increasing finding of drug-resistant microorganisms [2]. Antibiotics are the most frequently used pharmaceuticals. Levofloxacin (LFX) (Figure 1) is a third-generation fluoroquinolone antibiotic that is highly successful in treating severe bacterial infections, osteomyelitis, and other diseases [3]. Among the pharmaceutical compounds, LFX appears as the antibiotic most commonly detected in surface water and waste water at $ng \cdot L^{-1}$ levels [4]. In addition, the human body can only metabolize 15% to 20% of LFX; the other component is excreted [5]. The presence of LFX in the aquatic environment leads to the development of antibiotic-resistant genes (ARGs). Furthermore, LFX has been shown to be hazardous to certain aquatic species, endangering the ecosystems supporting marine life [6]. Thus, it is critical to remove LFX from aquatic environments in order to enhance public health and aquatic ecosystem safety.

The techniques reported for the elimination of LFX, such as adsorption [7], biological technique [8], electrocatalytic [9], activated sulphate [10], and photocatalysis [1, 3, 6, 11]. Among various method, the photocatalyst method is widely

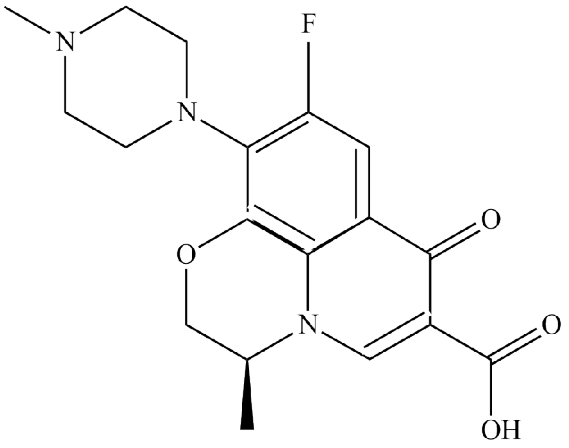

Figure 1. Levofloxacin chemical structure

regarded as a very profitable technology for removing contaminants due to its exceptional efficiency and the simplicity and reusability of its procedures [12]. Photocatalytic technology has been widely employed by researchers for the degradation of LFX. The photocatalyst efficiently decomposes LFX by producing hydroxyl radicals $(\cdot OH)^-$ more and radicals of superoxide (O_2^-) [13].

The development of photocatalysts driven by visible-light is essential for visible-light utilization. Bi-based semiconductors have been developed due to the distinctive structure of bismuth, whose compounds readily form layered structures and are responsive to visible light. Bismuth oxide (Bi_2O_3) is a basic semiconductor composed of bismuth, with a band gap energy ranging from 2.1 through 3.9 eV, it has been widely used in catalysts [14]. In order to facilitate photocatalysis, Bi_2O_3 effectively absorbs visible light, producing electron-hole pairs that aid in the degradation of contaminants [15]. In addition to heterogeneous photocatalysis, the semiconductor Bi_2O_3 has been implemented in thin films [16–18] and nanoparticles [19–21], among others.

Thin films photocatalysts have garnered significant interest due to their straightforward preparation, cost-effectiveness, ability to be applied to various substrates, and environmentally beneficial nature. Furthermore, thin films offers numerous benefits in comparison to powders, including less agglomeration and enhanced catalytic activity without the need for large quantities of ingredients [22]. The characteristics of Bi_2O_3 thin films can be controlled through synthesis techniques [23]. Several technique have been employed to enhance the characteristics of Bi_2O_3 thin films such as magnetron sputtering [24], chemical vapor deposition (CVD) [25], pulsed laser deposition (PLD) [26], spray pyrolysis [27], and sol-gel [28]. Utilizing the sol-gel method to create new materials, especially oxide-based coatings, has attracted a lot of scientific attention in recent years. This method is especially useful for producing thin films with strong control over composition and microstructure due to the gentle synthesis conditions [29].

Sahoo and Panigrahi, reported that Bi_2O_3 doped graphene obtained by modified sol-gel technique [28]. Xiaohong et al. discovered that Bi_2O_3 thin films, produced by the sol-gel method and coated using a dip-coating technique, demonstrated photocatalytic activity in the degradation of Rhodamine B [30]. Ilsatoham et al. also showed that Bi_2O_3 thin films fabricated using the sol-gel technique. The sol-gel process, when combined with spray coating, has several advantages over other regularly employed techniques for preparing Bi_2O_3 thin films. These advantages include user-friendly interface, meticulous regulation of chemical composition, cost-effective machinery, deposition at low temperatures, and the capability to generate superior films in diverse forms and dimensions [31]. Consequently, this methodology is being employed as a promising and feasible method for synthesizing materials.

Doping Bi_2O_3 thin films with metal ions, such as copper (Cu), can enhance their performance. The selection of the Cu element was based on its widespread utilization in metal-doped semiconductor photocatalysts. In addition, the atomic number of copper (Cu) is relatively smaller than that of bismuth (Bi), which aids in the ion replacement process [32]. There is a limited amount of literature available on Cu doping Bi_2O_3 (CBO) thin films. Hence, this work intended to investigate the influence of Cu doping on the structural and optical properties of Bi_2O_3 thin films. The films were produced using the sol-gel process and applied onto a glass substrate using spray coating. The structural analysis involves examining the formation of phases and the degree of crystallinity in of CBO thin films. The study of optical qualities encompasses the analysis of spectra and the determination of bandgap energy. Furthermore, the study examines the photocatalytic efficiency of the produced CBO thin films in the breakdown of LFX antibiotic contamination.

MATERIALS AND METHOD

Materials

Bismuth (III) nitrate, Bi $(NO_3)_3 \cdot 5\ H_2O$, copper (II) nitrate Cu $(NO_3)_3 \cdot 3H_2O$ were purchased by Sigma Aldrich company and used as a Bi and Cu precursor. Sodium hydroxide (NaOH), nitric acid (HNO_3), and Ethylene glycol were purchased by Merck KGaA as a solvent. The solutions were prepared using deionized water. The solvents utilized for CBO thin films deposition include acetone, methanol, and deionized water. The CBO thin films were utilized during the application step of LFX. The Levofloxacin Hemihydrate tablets were obtained from a local pharmaceutical company in Semarang, Central Java, and subsequently prepared to be used as the LFX stock solution.

Preparation of CBO thin films

CBO thin films were produced via the sol-gel procedure and coated using the spray coating technique. According to Figure 2, the CBO precursor needs to be prepared beforehand. The process of creating a CBO precursor operates as follows: 500 mg of bismuth nitrate was dissolved into 50 mL of 5% HNO_3, stirred for 10 minutes at room temperature to ensure uniformity. Subsequently, copper nitrate was added into the uniform solution, exhibiting concentration variations of 0, 1, 3, 5, and 7%. In addition, the mixture was uniformly blended for a duration of 10 minutes at room temperature using a stirrer set at a speed of 500 rpm. Afterwards, 250 mL of NaOH was poured into the homogeneous solution, and stirred for a duration of 2 hours. After allowing the solution to stand and form a suspension, the precipitate was isolated. The precipitate was once again dissolved in 50 mL of 5% HNO_3 and adding 10 mL of ethylene glycol. The solution is heated on a hotplate at a temperature of 175 °C for a period of 30 minutes, with simultaneous stirring at a speed of 670 rpm, resulting in the formation of a transparent and uniform mixture. Subsequently, a transparent solution will be used to a CBO thin films deposition.

The CBO thin films were deposited utilizing the spray coating method. Spray coating is a technique where a pressurized gas flow has been utilized to push tiny particles of coating material onto a surface, known as a substrate. The CBO precursor solution will be spread over a glass substrate that has been prepared and has dimensions of 25.4×76.2 mm and a thickness of 1–1.2 mm. The glass substrate conducted a methodical cleaning process utilizing liquid acetone, methanol, and aqueous solutions for a duration of 15 minutes. Next, the substrate's glass was heated to a temperature of 450 °C. for a duration of 30 minutes. This procedure has been performed relying on prior research completed by Ilsatoham et al. [31]. Next, about 50 mL of the CBO precursor

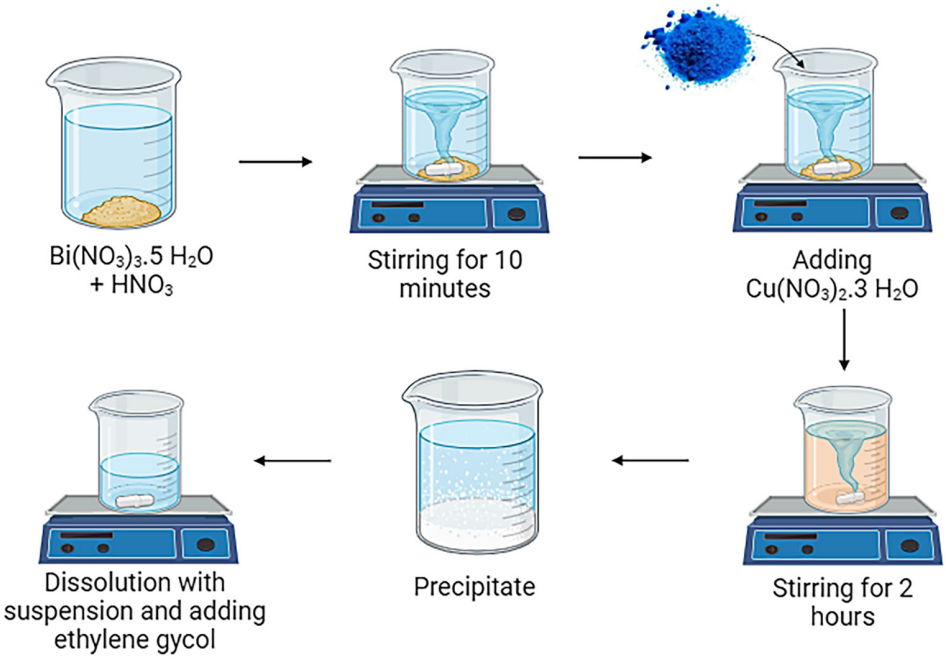

Figure 2. Preparation of precursor for CBO thin films

solution was applied over a glass substrate with a separation interval of approximately 30 cm. The deposition process was conducted perpendicularly using an airbrush sprayer, as depicted in Figure 3. Following the deposition procedure, the temperature of the hotplate was systematically reduced to create a uniformly thin films that does not develop any cracks. The CBO thin films were thereafter subjected to annealing in a furnace at a temperature of 350 °C for a duration of 2 hours.

Characterization of CBO thin films

The CBO thin films were analysed using CBO thin films characterization techniques to evaluate its crystal structure, composition, shape, and optical characteristics. The initial study of the CBO thin films was conducted using the spectrophotometer ultraviolet-visible (UV-Vis) (Flame, Ocean Optics). The optical features of CBO thin films were assessed using UV-Vis spectra, which measured wavelengths ranging from 200 to 1000 nm. Subsequently, the band gap energy values of the CBO thin films were determined using the Tauc plot approach. Further, it was subjected to X-ray diffractometer (XRD) instrument (Shimadzu 7000 type) for structural analysis and crystal phase with Cu-K α_1 radiation with angular range from 0.02° to 2θ, and from 20° to 60°.

Photocatalytic study of LFX degradation

The photocatalytic activity of CBO thin films was assessed by measuring the degradation of LFX in the presence of UV radiation. A stock solution of LFX was prepared specifically for LFX tablet with a concentration of 50 mg/L (50 ppm). LFX solution was homogenized using ultra-turra with a stirring speed at 450 rpm for 30 min. Each prepared sample was placed into a 50 mL of LFX solution. The experiment was conducted within an enclosed box that was supplied with a UV-C lamp (Philips TUV-30-W, 265 nm, Netherlands) operating at the room temperature. To ensure uniform lighting for the solution, the UV-C light was placed in the middle of the sample. Before activating the UV-C lamp, the LFX solution was permitted to remain undisturbed for a duration of 30 minutes in order to attain a state of adsorption equilibrium, thereby ensuring that solely photocatalytic activity occurred throughout the experiment. Subsequently, the LFX solution is placed under irradiation for a period ranging from 0 to 5 hours, during which the LFX concentration is assessed at 30-minute intervals. The concentration of the LFX solution was evaluated during the photodegradation process using a UV-VIS spectrophotometer, along with its corresponding absorption spectra before and after treatment. Degraded LFX concentration was calculated using the formula (Eq. 1) [33].

$$Degradation\ (\%) = \frac{C_o - C_t}{C_o} \times 100\% = \frac{A_o - A_t}{A_o} \times 100\% \quad (1)$$

where: C_o represents the starting concentration of LFX (mg/L), C_t represents the concentration of LFX at certain time (mg/L), A_t represent the absorbance of LFX at different times (a.u), and A_o is the blank absorbance of the original solution (a.u).

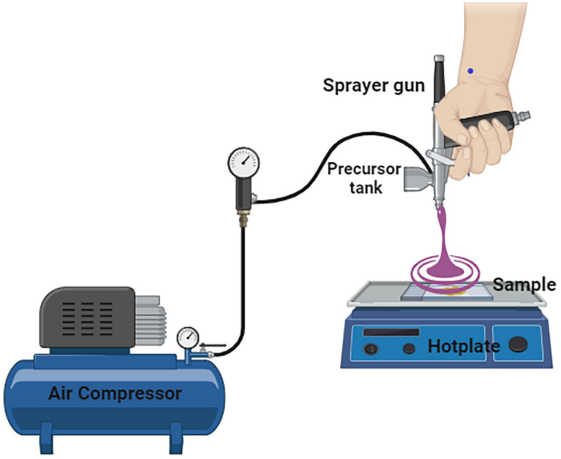

Figure 3. Schematic of the spray-coating technique for CBO thin films deposition

Degradation kinetics of LFX

The proposed model for photocatalytic activity aims to offer a more rigorous methodology for the degradation of LFX. Subsequently, the kinetic model was used to evaluate the degradation kinetics of LFX. Equation 2 and 3 displays the mathematical equations of the kinetic model, which consist of pseudo-first-order and pseudo-second-order kinetic models.

$$ln\frac{C_t}{C_o} = -k_1.t \quad (2)$$

$$\frac{1}{C_t} - \frac{1}{C_o} = k_2.t \quad (3)$$

where: k_1 – represent the rate constant of pseudo-first-order kinetics, and k_2 – represent the rate constant of pseudo-second-order kinetics.

RESULTS AND DISCUSSION

Visual characteristic of CBO thin films

The synthesis of CBO thin films was effectively achieved by the sol-gel method, and they were then put onto a glass substrate utilizing spray-coating procedures. Figure 4 displays the surface colour of CBO thin films at different concentrations of Cu doping. The Pure Bi_2O_3 was completely formed, as evidenced by the yellow hue of the product. As an increasing concentration of Cu is introduced into Bi_2O_3, a progressive transition in surface colour from green to brown transpiration is observed. When blue dissolved Cu nitrate is combined with yellow dissolved Bi nitrate, colour shifts occur; as a result, the surface colour will turn green and brownish in the opposite direction.

It corresponds to Le Chatelier's Principle, which examines the impact of varying conditions on a system in equilibrium. The addition of coloured ions to a process will result in the formation of a darker compound. Mendoza et al. also documented the phenomenon of colour change resulting from the systematic integration of Cu, leading to a darker hue of the material. The colour transitions from a subtle shade of grey to a subtle shade of brown [34]. Hemathangam et al. also reported the addition of Cu at high concentrations results in a darker discoloration of thin films [35].

Optical study

The study of CBO thin films for LFX degradation places considerable focus on the optical characteristics, including as transmission, absorption, and energy gap. Figure 5 displays the optical transmittance curves at various concentrations as a function of wavelength. The optical transmittance spectra of the pure Bi_2O_3 and CBO thin films were measured in the wavelength range of 200 to 1000 nm. The transmittance of pure Bi_2O_3 is around 40%. The transmittance of CBO thin films decreases from 25% to 5% when the Cu doping concentration increases from 1% to 5%. However, when the Cu concentration reaches 7%, the transmittance increases again to 30%. The transmittance spectrum exhibits a contrasting pattern to the absorption spectrum, indicating the comparatively low transmittance of CBO thin films in comparison to pure Bi_2O_3. The decrease in transmittance observed in CBO thin films can be attributed to the enhanced crystallization process. The decrease in transmittance of the CBO thin films was attributed to the scattering of light on their rough surfaces, which occurs as the grain size increases. Another observation about these transmittance spectra is the shift of the absorption edge towards longer wavelengths. The changes in absorption and transmission can be ascribed to the variation in thickness and the fundamental variations in the absorption characteristics of the CBO thin films [35].

Figure 6 exhibits the optical absorption spectra of undiluted Bi_2O_3 and CBO thin films at room temperature, spanning a wavelength range from 200 to 1000 nm. The absorbance spectra of

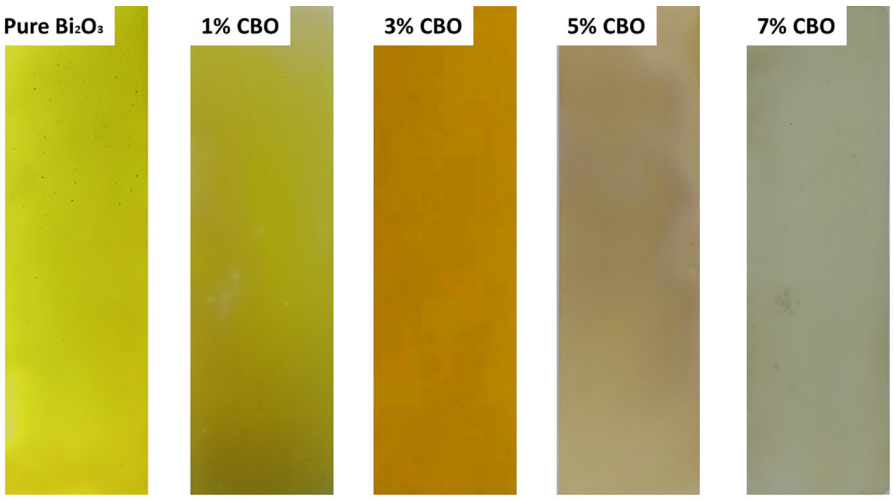

Figure 4. Visual characteristics of the CBO thin films

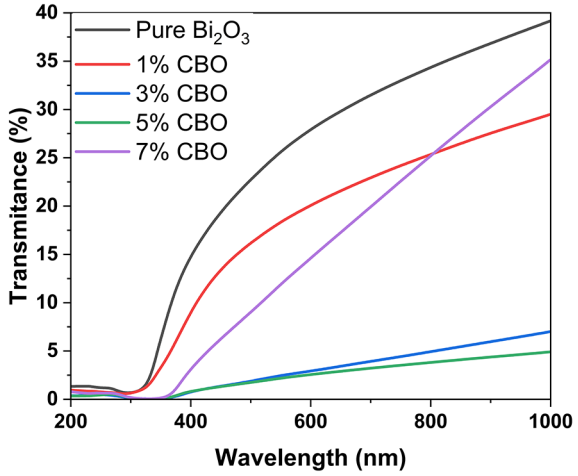

Figure 5. The transmittance spectra of CBO thin films

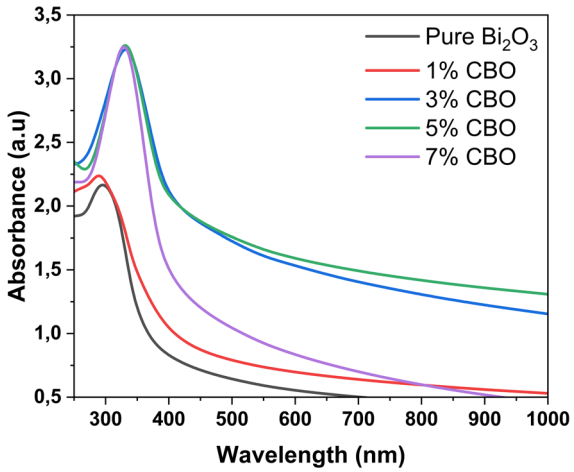

Figure 6. The absorbance spectra of CBO thin films

pure Bi_2O_3 have distinct peaks at a wavelength of 295 nm, which are observed to be the minimum and progressively grow with the addition of Cu to Bi_2O_3. The UV-Vis spectra of undiluted and copper-doped bismuth oxide thin films display a discrepancy in the wavelength of the peaks corresponding to the maximum absorption.

The addition of copper (Cu) into the Bi_2O_3 thin films results in an enhancement of the optical absorption properties, as well as a displacement of the optical absorption maximum towards the higher wavelength range spanning from 295 nm to 330 nm. With an increase in Cu concentration, there will be a corresponding increase in the absorption coefficient. The results indicate a rise in the optical band gap. The highest absorption coefficient was observed at a concentration of 3% CBO, measuring 3.2485 average units (a.u.), and exhibited a progressive reduction from 5% CBO to 7% CBO. The creation of hole carriers after the addition of Cu doping is the fundamental source of this phenomena, which results in the Femi level transitioning into the valence band and aligning with the density of states [36]. The observation reveals that an increase in Cu doping leads to a more pronounced alteration in the absorption spectrum. The obtained calculations align with the band gap analysis described below, which is in accordance with the experimental findings.

The energy band gap is a crucial optical property that plays a significant role in defining a material's photocatalytic capacity. The addition of copper to the Bi_2O_3 element will greatly modify its photocatalytic bandwidth, consequently impacting the range of responses exhibited by the photocatalyst under visible light. This alteration enables the photocatalyst to absorb visible light across different wavelengths, ultimately influencing its catalytic activity. Subsequently, it is imperative to examine the level of Cu doping in the Bi_2O_3 photocatalyst, as the degree of Cu doping in the crystal structure of Bi_2O_3 does not exhibit a direct correlation with its capacity to modify UV-vis light absorption and bandwidth gap. The optical band gap value (E_g) of samples have been calcuated by fitting the absorption data using Tauc-plot equation,

$$\alpha h\nu = A\,(h\nu - E_g)^n \tag{4}$$

Many factors determine the absorption coefficient, represented by α, v is the frequency of the incoming photon, E_g represents the band gap energy value, and n is a value that is equal to 1/2 for a direct band gap and 2 for an indirect band gap compound, A is an energy-independent constant, and h is Planck's constant.

The energy band gap of pure Bi_2O_3 is determined to be 3.05 eV through measurement. The introduction of varying amounts of Cu (1%, 3%, 5%, and 7%) led to a reduction in the energy band gap, with values of 2.93, 2.54, 2.62, and 2.83 eV correspondingly. An increase in the amount of Cu element leads to a decrease in the band gap value, which in turn enhances the optical activity. The minimum energy band gap was obtained by CBO 3%, which is 2.54 eV. A small energy band gap indicates a decrease in the breadth of the energy band gap between the valence band and the conduction band. UV light irradiation induces excitation, hence lowering the energy threshold for electron transfer from the valence band to the conduction band. This enables the generation of

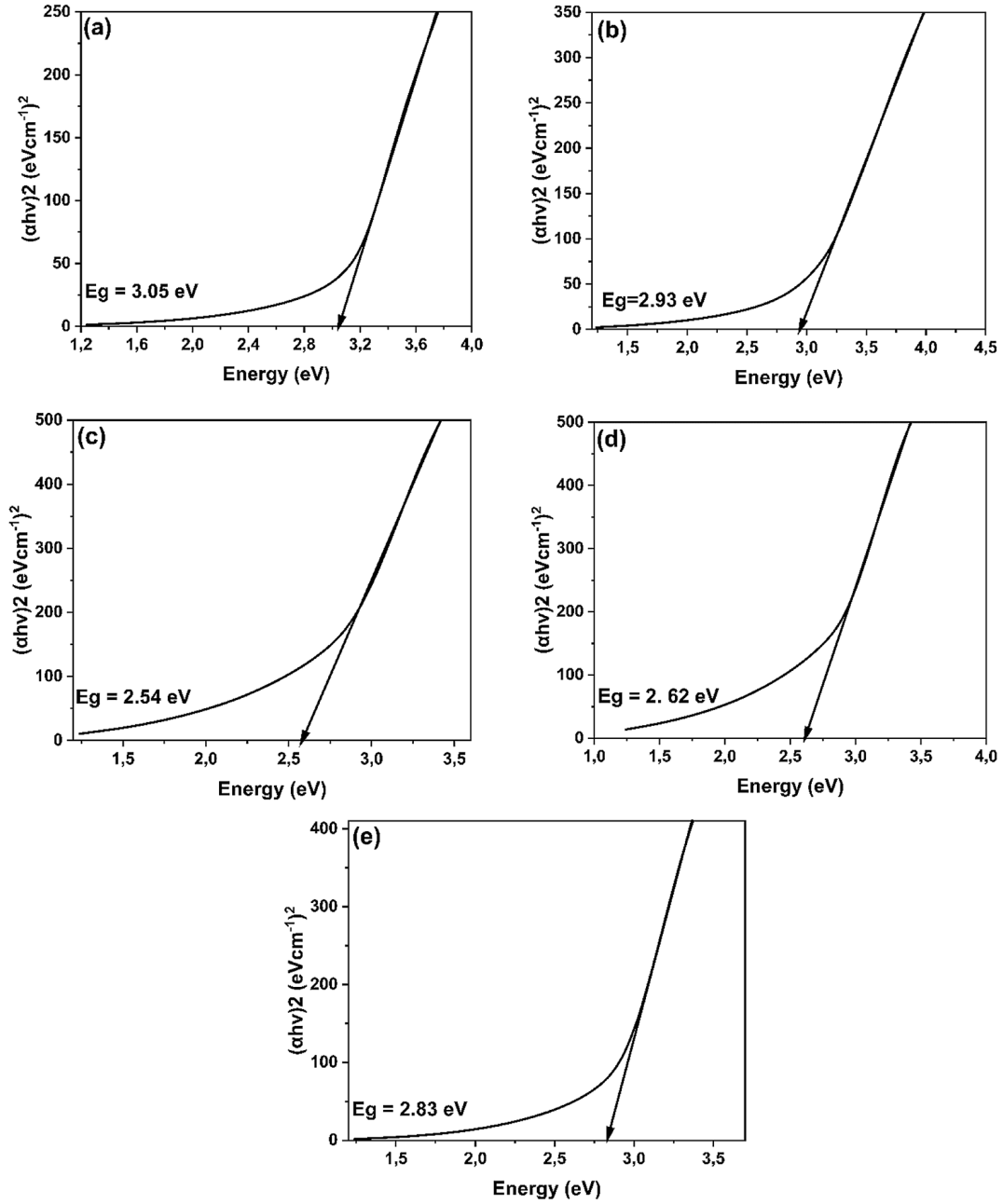

Figure 7. The bandgap energy plot of thin films: (a) pure Bi_2O_3, (b) 1% CBO, (c) 3% CBO, (d) 5% CBO, and (e) 7% CBO

electrons and holes. Enhancing the photocatalytic activity can be achieved by generating a greater number of electrons and holes.

Structural analysis

The XRD pattern is used to determine the crystal microstructure of the resulting samples. In Figure 8(a) shows the full spectrum of XRD for pure Bi_2O_3 and 1%, 3%, 5%, and 7 % CBO thin films between 20° and 80°. Figure 8b displays the XRD spectra of pure Bi_2O_3 and CBO thin films. As shown in Figure 8b the pure Bi_2O_3 thin films exhibit seven major diffraction peaks at 2θ: 27.88°, 31.67°, 32.68°, 46.17°, 46.91°, 54.22°, and 55.49° which matched with miller index (201), (002), (220), (222), (400), (203), and (421). The XRD pattern of pure Bi_2O_3 thin films closely matches the structure of Bi_2O_3 (pdf data card number ICDD-00-027-0050), showing the process of creating a singular phase of Bi_2O_3. The pure Bi_2O_3 thin films corresponds to tetragonal Bi_2O_3 (β-Bi_2O_3) with space group p-421c and lattice parameters such as *a* = *b*: 7.742 Å, c: 5.631

Å, $\alpha = \beta = \gamma$: 90°, and cell volume: 337.51 Å^3. Using the XRD data and Equation 5, the lattice parameter an of a tetragonal Bi_2O_3 structure was determined.

$$\frac{1}{d^2_{(hkl)}} = \frac{h^2+k^2+l^2}{a^2} \quad (5)$$

where: a – lattice parameter, d_{hkl} – the inter-plane spacing, and h, k, and l are the indices of the planes.

Interestingly, the introduction of Cu doping upon CBO thin sheets results in the appearance of a new phase at 2θ: 25.74°, 29.23°, 29.92°, and 47.98° with miller index (210), (211), (002), and (410) as shown in Figure 8b. The doping of Cu in the CBO thin films affects the sample's parent phase, this results in the emergence of supplementary diffraction peaks linked to copper or copper oxide. The presence of Cu-doped Bi_2O_3 can be classified as a surface or interface phenomenon. The intensity of all the planes exhibits an upward trend as the copper concentrations increase from 1% to 3%. However, after 3% copper concentration, the intensity starts to decline. These findings align with prior research indicating that the addition of copper at a concentration of 3–4% led to a reduction in diffraction intensity [37], [38].

The result of 3% CBO thin films based on XRD pattern corresponds to Copper Bismuth Oxide ($Bi_{7.38}Cu_{0.62}O_{11.69}$) phase according to pdf data card number ICDD-00-049-1765. No peaks indicating impurities were seen in the patterns, confirming the formation of pure Cu-Bi_2O_3 (CBO). Overall, the diffraction peaks exhibit sharpness and a consistent baseline. The data suggests that the presence of 3% CBO thin sheets significantly impacts the crystal structure. The lattice parameters value of 3% CBO thin films are a=b: 7.7365 Å, c: 5.6324 Å, α=β=γ: 90°, and cell volume: 337.12 Å^3. The size of the crystallite (D_s) was determined using the Debye-Scherrer formula. Additionally, the lattice parameters, dislocation density (δ), and microstrain (ε) were also calculated and presented in Table 1. The formulae provided were used to examine the crystallite size, dislocation density, and microstrain.

$$D_s = \frac{k\lambda}{\beta cos\theta} \quad (6)$$

$$\delta = \frac{1}{{D_s}^2} \quad (7)$$

$$\varepsilon = \frac{\beta}{4tan\theta} \quad (8)$$

where: D_s – crystallite size (nm), k = 0.94 represents the Scherrer constant, λ = 1.5406 Å represengts the X-Ray wavelength, β – the full width and half maximum (FWHM), θ – the Bragg angle diffraction peak in radians, δ – dislocation density (line/m^2), and ε – microstrain (e).

The pure Bi_2O_3 has a crystallite size of 15.0779 nm. Upon increasing the concentration of Cu from 1% to 3%, the crystallite size exhibited an increase to 22.8398 and 28.1938 nm, respectively. The 3% CBO has the smallest FWHM value of 0.2856 and the largest crystal size of 28.1938 nm. In addition, the size of the crystallites decreased further when 5% and 7% of Cu was added. The inclusion of Cu led to variations in the crystallite size. The better crystallinity was shown by the smaller FWHM value, which indicates that it is simpler for nearby atoms to change the length and orientation of their bonds.

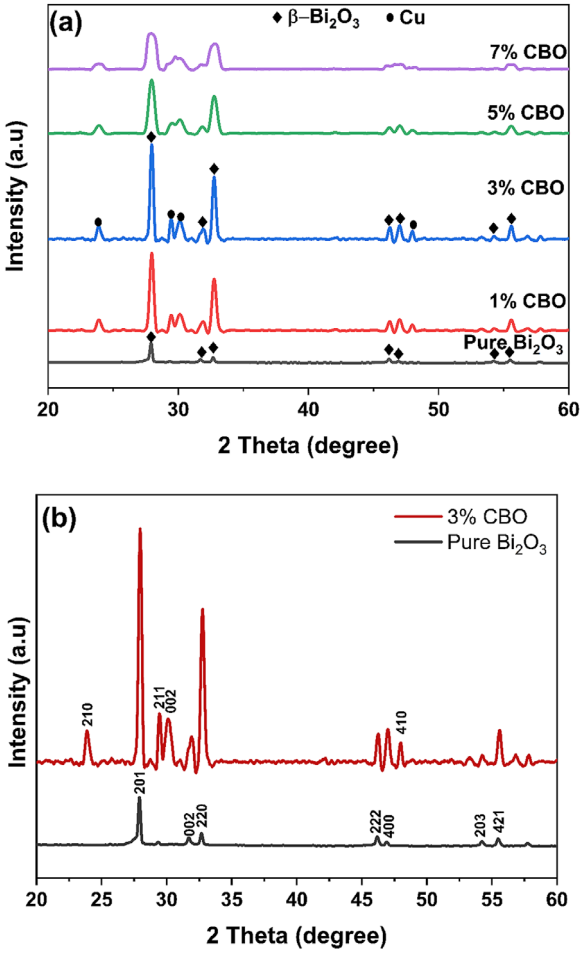

Figure 8. (a) Full spectrum of XRD, and (b) detailed XRD diffractogram pattern of pure Bi_2O_3 and 3% CBO thin films

Increasing the amount of Cu doping in Bi_2O_3 leads to an increase in the capacity of the unit cell and crystallite size. However, this can disrupt the arrangement of atoms and the stability of Bi_2O_3. The disparity in size and charge between Cu and Bi ions can lead to chain distortions and flaws in materials [39]. The addition of a small amount of Cu to Bi_2O_3 (1% CBO) causes a disturbance in its crystal structure as a result of disparities in ion sizes. This results in the formation of imperfections, impeding the process of crystal growth and leading to a reduction in size [40]. It is evident that there is an inverse relationship between the FWHM and the size of the crystallite. As the FWHM decreases, the size of the crystallite grows. Nevertheless, both the dislocation density and micro strain see a decrease. Defects in the material can be detected by analyzing the dislocation density and micro strain. The presence of these flaws in the CBO can lead to a reduction in the photocatalytic efficacy of antibiotics. From the outcome, it is evident that the 3% CBO thin films were expected to exhibit good photocatalytic activity.

Levofloxacin degradation performance

The study examined the efficacy of a photocatalyst produced using pure Bi_2O_3 and CBO thin films in degrading LFX. Doping Cu into the Bi_2O_3 photocatalyst will have a substantial impact on its bandgap, thus altering the range of light that the photocatalyst can respond to. This modification enables the photocatalyst to absorb UV light within various wavelengths, ultimately influencing its catalytic activity. The process entailed the degradation of LFX, which had an initial concentration of 50 parts per million (ppm). The photocatalytic activity was evaluated by periodically measuring the absorbance at a specified wavelength (290 nm) while exposing it to UV radiation. The degradation efficiency was measured by monitoring the variation in absorbance at a wavelength of λ_{max} = 290 nm. The evaluation of the effectiveness of degradation was a pivotal result of this study.

Figure 9 demonstrates that the 3% CBO thin films exhibited the best degrading efficiency, compared with pure Bi_2O_3 and variation of concentration CBO thin films. In the absence of Bi_2O_3 thin films, we observed minimal degradation of levofloxacin throughout our photolysis and photocatalysis tests. The photolysis of LFX was also studied at same conditions but without the presence of catalyst. The lack of a catalyst resulted in a small decrease of 9.13% in LFX concentration over a period of 5 hours, suggesting that photodegradation was insignificant. The results suggest that the photolysis process only using UV irradiation is not efficient for the degradation of LFX. This process occurs when photocatalysts are added to the matrix, leading to changes in the catalyst structure and the initiation of photocatalytic reactions on the catalyst surface.

CBO thin films exhibit a higher photocatalytic activity compared to pure Bi_2O_3. The degradation efficiency for a 5-time photocatalytic process utilizing different concentrations of CBO thin films (pure Bi_2O_3, 1%, 3%, 5%, and 7%) is as follows: 46.93%, 75.21%, 85.95%, 79.34%, and 68.97%, respectively. The results indicated that

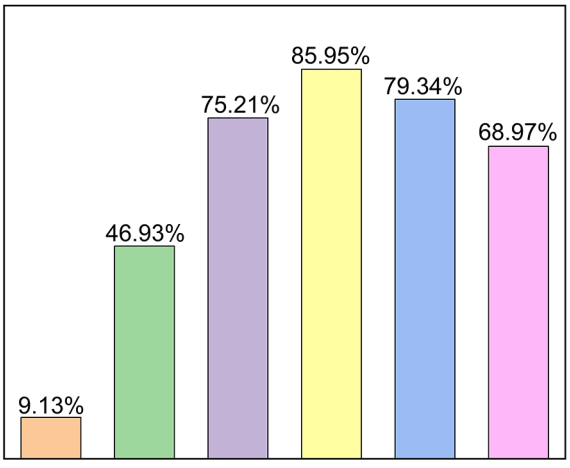

Figure 9. Levofloxacin degradation efficiency

Table 1. Computed crystallographic parameters for Pure Bi_2O_3 and CBO thin films

Sample	2θ (°)	FWHM (β)	Crystallite size (nm)	Dislocation density (line/m^2) x 10^{-3}	Microstrain (e) x 10^{-3}
Pure Bi_2O_3	27.8795	0.5341	15.0779	4.3986	9.3888
1% CBO	29.95932	0.3509	22.8398	1.9169	5.7229
3% CBO	27.961	0.2856	28.1938	1.2580	5.0050
5% CBO	27.95432	0.5004	16.0892	3.8630	8.7728
7% CBO	27.95143	0.7005	11.4949	7.5681	12.2805

the addition of Cu altered the degrading activity of the Bi2O3 catalyst. The thin films with a 3% concentration of CBO exhibit the highest level of degrading efficiency. This is a result of the predominant synergistic effects caused by Cu^{2+} ions.

The inclusion of Cu^{2+} ions increased the quantity of active sites on the catalyst and reduces the rate at which holes and electrons combine again, therefore improving the photocatalytic efficiency of CBO thin films. The activity of the catalyst may be influenced by the various constituents present in Cu doped Bi_2O_3 thin films, maybe due to the specific surface area of the synthesised CBO thin films [41]. The findings demonstrate that the inclusion of Cu in Bi_2O_3 thin films at concentrations of up to 3% enhances photocatalytic activity. However, exceeding this threshold of 3% Cu concentration leads to a decline in photocatalytic activity. At higher concentrations, the presence of particles acts as a barrier, creating a mask on the photosensitive surface. This barrier obstructs or reflects the passage of light, preventing photons from reaching the antibiotic's surface [42].

Figure 10 demonstrates a notable reduction in the absorption intensity of LFX as the duration of UV irradiation increases. Increasing the length of irradiation resulted in the formation of a higher number of degrading species from the active Bi and Cu^{2+} photocatalyst, resulting in a bigger concentration of degraded LFX. According to the results, the initial reduction in LFX concentration was remarkably significant, suggesting that the antibiotic underwent fast degradation. Nevertheless, the rate of reaction decelerates over time and ultimately achieves its minimum velocity. During the initial stages of the testing, it is clear that there are a significant number of empty areas on the catalyst surface. The number of active sites initially grows and thereafter decreases progressively over time. After approximately 210 min, the rate of degradation becomes consistent in the state of equilibrium and enters a stable state. Therefore, the highest level of degradation of LFX occurs after 210 min when exposed to UV light and catalyst, making it the most favourable time for degradation.

Antibiotic concentrations decrease when LFX breaks down into CO_2 and H_2O. This is caused by a degradation process between LFX and hydroxyl radicals (·OH), which are created from the decomposition of H_2O molecules upon the absorption of UV photons (hv). The chemical process of photolysis is as follows due to the presence of only the UV and LFX reaction:

$$H_2O + hv \rightarrow \cdot OH + H^+ + e^{-z} \quad (9)$$

The generation of ·OH radicals in the photolysis reaction is somewhat challenging, leading to limited ·OH radical production. The slow degradation process of LFX results in a low percentage of degradation. In the photocatalytic process, however, the presence of CBO thin films makes the ·OH radical formation process more involved in the degradation of LFX, resulting in

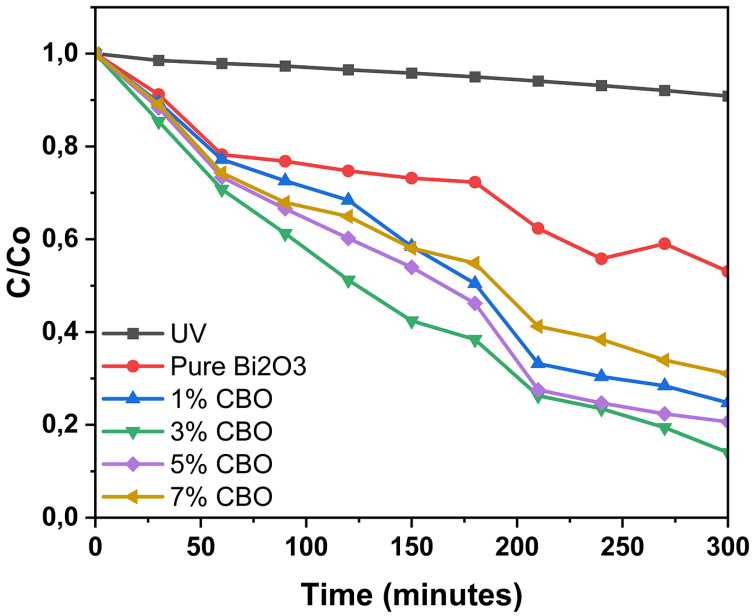

Figure 10. Absorbance decrease graph of LFX

an enhanced degradation of LFX. In order to elucidate the impact of CBO thin films on the photocatalytic process, the mechanism of photocatalysis was considered. Typically, the photocatalytic process begins when CBO thin films are exposed to UV-light possessing energy equal to or greater than the band gap energy of CBO thin sheets. UV light irradiation caused excitation of electrons from the valence band to the conduction band in CBO thin films.

The act of stimulating an electron from the valence band to the conduction band leads to the creation of an electron-hole pair, as illustrated in the subsequent equations. The ·OH radicals, hydrogen ions (H^+), and hydrogen peroxide (H_2O_2) were generated through the reaction of water molecules with the hole (h^+). The H_2O_2 generated during the reaction underwent decomposition into two ·OH radicals, which were mainly accountable for the degradation of LFX. The conduction band enabled the generation of superoxide radicals ($\cdot O_2^-$) by involving electrons. The H_2O_2 molecule was synthesized by mixing them, due to the high reactivity of reactive oxygen species (ROS). The degradation of ciprofloxacin occurred due to the disintegration of the H_2O_2 molecule into ·OH radicals. The mechanism depicting the degradation of LFX through active species is shown in Figure 11.

The kinetics of the catalytic elimination of LFX using bismuth oxide thin films were analyzed using the pseudo-first order and second order models. Figure 12a and 12b show graphs of the natural logarithm of the ratio of

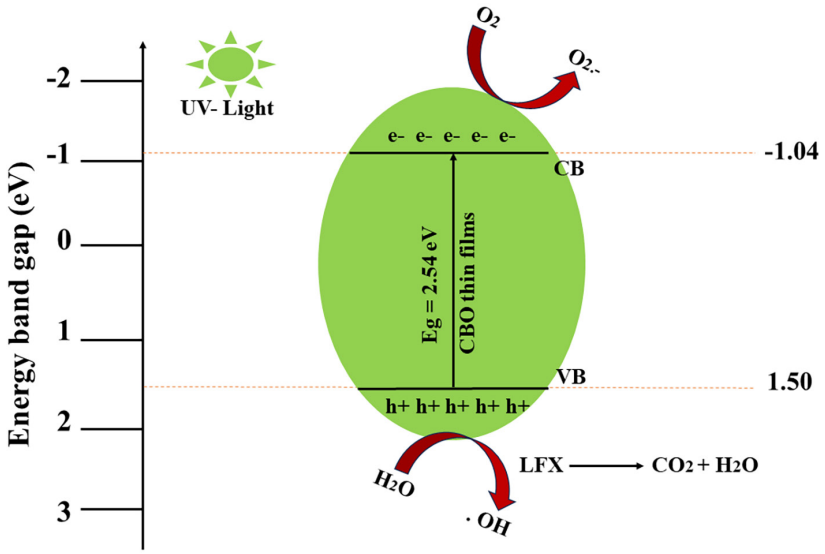

Figure 11. Mechanism for the degradation of LFX

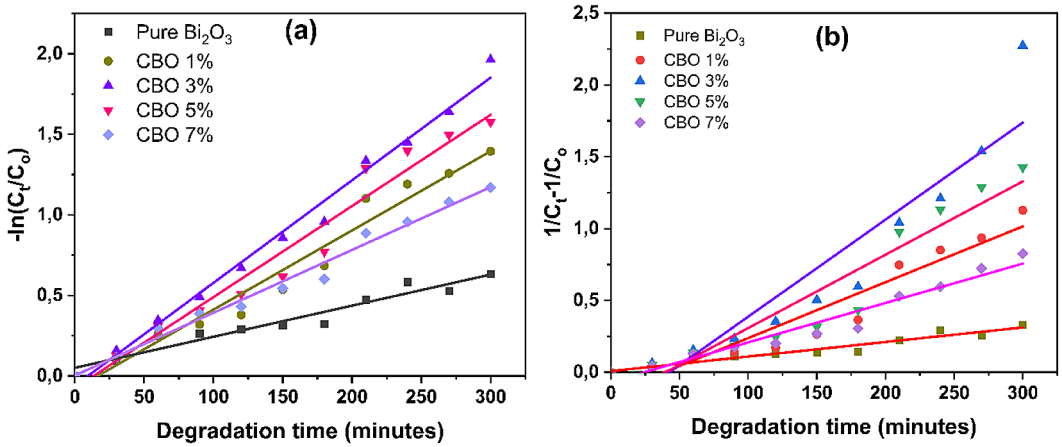

Figure 12. Levofloxacin degradation results following by (a) pseudo-first-order kinetics, and (b) pseudo-second-order kinetic

Table 2. Kinetic rate constant for degradation of LFX

Sample	First-order-kinetics		Second-order-kinetics	
	k (min^{-1})	R^2	k (min^{-1})	R^2
Pure Bi_2O_3	0.00193	0.9389	0.00101	0.9354
1% CBO	0.00492	0.9642	0.00389	0.9138
3% CBO	0.00637	0.9897	0.00676	0.8809
5% CBO	0.00566	0.9633	0.00511	0.9051
7% CBO	0.00389	0.9842	0.00274	0.9511

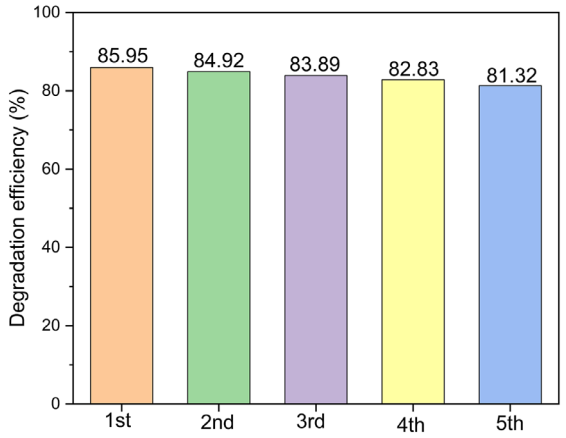

Figure 13. Photocatalytic stability of 3% CBO thin films with LFX solution

concentration at time t to the initial concentration (*ln* (*Ct*/*Co*)) plotted against time, and the reciprocal of the difference between the concentration at time t and the initial concentration (1/*Ct*-1/*Co*) plotted against time, respectively. The rate constant for the degradation of LFX, along with k (rate constant) and R^2 are listed in Table 2. The kinetic data indicate that the degradation of LFX corresponds to the first pseudo-order model rather than the second order model. This is supported by the higher R^2 values seen for the first order, suggesting that the degradation process is more efficient.

Under similar conditions, thin films of CBO with a concentration of 3% exhibit the highest degrading rate constant. Specifically, the value is 0.00637 min^{-1} for pseudo-first-order kinetics and 0.00676 min^{-1} for pseudo-second-order kinetics. The degradation rate constant for pure Bi_2O_3 thin films is 0.00193 min-^{1} and 0.00101 min^{-1} for pseudo first and second-order kinetics, respectively. The rate degradation refers to the rate at which a material breaks down LFX. A greater rate degradation number indicates a faster degradation of the material, resulting in a lower amount of LFX remaining in the material.

Photocatalyst stability test

The efficiency and reusability of a photocatalyst are crucial factors in the photocatalytic process. The stability of 3% CBO thin films was evaluated during five degradation experiments using a solution containing 50 parts per million (ppm) of LFX. The concentration of LFX and the degree of degradation yielded significant insights into the degradation experiment. Following each cycle, the thin films were washed with deionized water to remove any LFX solution that had been absorbed on their surface, and then dried. The thin films were utilized in the second cycle without any application of heat. Figure 13 illustrates the enduring durability of the 3% CBO thin films, even after undergoing 5 cycles of regeneration.

The thin films in degrading LFX decreased the degradation efficiency from 85.95 % (1st cycle), 84.92% (2nd cycle), 83.89% (3rd cycle), 82.83% (4th cycle), and 81.32% (5th cycle). The decrease in degradation effectiveness is attributable to the diminishing number of active sites on the surface of the photocatalyst, which occurs after multiple usage and leads to alterations in the structure and characteristics of the thin films [43]. A gradual decrease in the degrading efficiency of thin films was observed, a phenomenon commonly encountered in catalysis. Nevertheless, the 3% CBO thin films exhibited excellent recyclability without any decrease in activity.

CONCLUSIONS

The study successfully fabricated and analysed various CBO thin films using advanced methods. The decreasing effectiveness of both pure Bi_2O_3 and all CBO thin films was examined in comparison to LFX solution in aquatic conditions. The liberated copper is considered to have a key role in the reduction in the energy band gap

CBO thin films during the process. The 3% CBO thin films have demonstrated superior degrading efficiency for LFX when exposed to UV radiation. The characterization results indicated that the thin films with 3% CBO exhibited the small est energy band gap, larger crystallite size, and broader range of sensitivity to UV light compared to the other samples. The purity of the synthesized composite was assessed using X-ray diffraction (XRD) analysis. The degradation efficiency of 3% CBO thin films using photocatalysis is 85.95%. The degradation kinetic rate value is 0.00637 min^{-1} for pseudo-first-order kinetics and 0.00676 min^{-1} for pseudo-second-order kinetics. The proposed mechanism for the enhanced degrading efficiency of the 3% CBO thin films has also been clarified. The thin films containing 3% CBO have exhibited exceptional reusability, even after experiencing five cycles of deterioration for LFX. This characteristic positions it as a highly probable candidate for environmental applications on a commercial scale. The addition of Cu to Bi_2O_3 enhances photocatalytic activity against LFX. It is inexpensive and environmentally safe, making it suitable for use in wastewater treatment materials.

Acknowledgment

This work was supported by The Ministry of Education, Culture, Research, and Technology of Republic Indonesia by PMDSU Batch VI Scheme with contract no.: 345-41/UN7.D2/PP/V/2024.

REFERENCES

1. Zhong X., Zou Z.S., Wang H.L., Huang W., Zhou B.X. 2019. Enhanced activation of persulfate by Co-doped bismuth ferrite nanocomposites for degradation of levofloxacin under visible light irradiation. Materials (Basel)., 12(23), 2019. doi: 10.3390/ma12233952.
2. Gong S., Sun Y., Zheng K., Jiang G., Li L., Feng J. 2020. Degradation of levofloxacin in aqueous solution by non-thermal plasma combined with Ag3PO4/activated carbon fibers: Mechanism and degradation pathways. Sep. Purif. Technol., 250(117264). doi: 10.1016/j.seppur.2020.117264.
3. Chen Z., Ning B., Cai Y., Liu M., Xu P., Zhang P., Xiao G., He Y. 2023. Rapid degradation of levofloxacin by p-n heterojunction AgFeO2/Ag3VO4 photocatalyst: Mechanism study and degradation pathway. J. Taiwan Inst. Chem. Eng., 151, 105126. doi: 10.1016/j.jtice.2023.105126.
4. Xia Y., Dai Q. 2018. Electrochemical degradation of antibiotic levofloxacin by PbO2 electrode: Kinetics, energy demands and reaction pathways. Chemosphere, 205, 215–222. doi: 10.1016/j.chemosphere.2018.04.103.
5. Hamad M.T.M.H., El-Sesy M.E. 2023. Adsorptive removal of levofloxacin and antibiotic resistance genes from hospital wastewater by nano-zero-valent iron and nano-copper using kinetic studies and response surface methodology. Bioresour. Bioprocess., 10(1), 1–29, 2023, doi: 10.1186/s40643-022-00616-1.
6. Go A.D., dela Rosa F.M., Camacho D.H., Punzalan E.R. 2022. Dataset on photocatalytic degradation of Levofloxacin using hydroxyapatite photocatalyst: Optimization by response surface methodology. Data Br., 42(February), 101126, 2022, doi: 10.1016/j.dib.2022.108219.
7. Go A.D., dela Rosa F.M., Camacho D.H., Punzalan E.R. 2022. Dataset on photocatalytic degradation of Levofloxacin using hydroxyapatite photocatalyst: Optimization by response surface methodology. Data Br., 42(January), 101126. doi: 10.1016/j.dib.2022.108219.
8. Ben Ayed A., et al. 2024. Genome sequencing of Porostereum spadiceum to study the degradation of levofloxacin. Ecotoxicol. Environ. Saf., 270(January). doi: 10.1016/j.ecoenv.2023.115808.
9. Wang S., et al. 2023. Electrocatalytic degradation of levofloxacin wastewater by Ru-Ti-Ni/CNT electrodes. Catal. Commun., 182(August), 106756. doi: 10.1016/j.catcom.2023.106756.
10. Lu X. et al. 2023. Levofloxacin degradation by porous Cox/CN activated peroxymonosulfate: Investigation of efficiency, mechanism, and degradation pathways. J. Water Process Eng., 56(October), 104427. doi: 10.1016/j.jwpe.2023.104427.
11. Nair N.G., Gandhi V.G., Modi K., Shukla A. 2024. Photocatalytic degradation of levofloxacin by GO-TiO2 under visible light. Mater. Today Proc., October. doi: 10.1016/j.matpr.2023.12.049.
12. Zhang M., et al. 2023. Preparation of BiVO4/CO32−-Bi2O2CO3 heterojunctions for enhanced photocatalytic activity in the degradation of levofloxacin under visible light. J. Alloys Compd., 965(July), 171471. doi: 10.1016/j.jallcom.2023.171471.
13. Sa'adah F., Sutanto H., Hadiyanto. 2022. Optimization of the Bi2O3/Cu synthesis process using response surface methodology as a tetracycline photodegradation agent. Results Eng., 16(June), 100521. doi: 10.1016/j.rineng.2022.100521.
14. Liu H.Z., Han Q.F., Ding H.W., Yu H.M., Chiu T.W. 2022. One-step route to α-Bi2O3/BiOX (X = Cl, Br) heterojunctions with Bi2O3 ultrafine nanotubes closely adhered to BiOX nanosheets. J. Taiwan Inst. Chem. Eng., vol. 131, 2022, doi: 10.1016/j.jtice.2021.11.014.

15. Long M., Hu P., Wu H., Cai J., Tan B., Zhou B. 2016. Efficient visible light photocatalytic heterostructure of nonstoichiometric bismuth oxyiodide and iodine intercalated Bi2O2CO3. Appl. Catal. B Environ., 184, 20–27. doi: 10.1016/j.apcatb.2015.11.025.
16. Medina J.C. et al. 2016. Sputtered bismuth oxide thin films as a potential photocatalytic material. Catal. Today, 266, 144–152. doi: 10.1016/j.cattod.2015.10.025.
17. Barrera-Mota K., Bizarro M., Castellino M., Tagliaferro A., Hernández A., Rodil S.E. 2015. Spray deposited β-Bi2O3 nanostructured films with visible photocatalytic activity for solar water treatment. Photochem. Photobiol. Sci., 14(6), 1110–1119. doi: 10.1039/c4pp00367e.
18. Correia F.C., Calheiros M., Marques J., Ribeiro J.M., Tavares C.J. 2018. Synthesis of Bi2O3/TiO2 nanostructured films for photocatalytic applications. Ceram. Int., 44(18), 22638–22644. doi: 10.1016/j.ceramint.2018.09.040.
19. Utami B.A., Sutanto H., Alkian I., Sa'Adah F., Hidayanto E. Efficient degradation of amoxicillin using Bi2O3/Fe synthesized by microwave-assisted precipitation method. Cogent Eng., 9(1), 2022, doi: 10.1080/23311916.2022.2119534.
20. Coronado-Castañeda R.R.S., M. L. Maya-Treviño, E. Garza-González, J. Peral, M. Villanueva-Rodríguez, A. Hernández-Ramírez. 2020. Photocatalytic degradation and toxicity reduction of isoniazid using β-Bi2O3 in real wastewater. Catal. Today, 341, 82–89. doi: 10.1016/j.cattod.2019.01.028.
21. Han S., Li J., Yang K., Lin J. 2015. Fabrication of a β-Bi2O3/BiOI heterojunction and its efficient photocatalysis for organic dye removal. Cuihua Xuebao/Chinese J. Catal., 36(12), 2119–2126. doi: 10.1016/S1872-2067(15)60974-3.
22. Chahkandi M., Zargazi M. 2020. New water based EPD thin BiVO4 film: Effective photocatalytic degradation of Amoxicillin antibiotic. J. Hazard. Mater., 389. doi: 10.1016/j.jhazmat.2019.121850.
23. Mane V., Dake D., Raskar N., Sonpir R., Stathatos E., Dole B. 2024. A review on Bi2O3 nanomaterial for photocatalytic and antibacterial applications. Chem. Phys. Impact, 8(January), 100517. doi: 10.1016/j.chphi.2024.100517.
24. Orozco-Hernández G., Olaya-Flórez J., Pineda-Vargas C., Alfonso J.E., Restrepo-Parra E., Structural, chemical and electrochemical studies of bismuth oxide thin films growth via Unbalanced Magnetron Sputtering. Surfaces and Interfaces, 21. Elsevier, 2020. doi: 10.1016/j.surfin.2020.100627.
25. Bandoli G., Barreca D., Brecacin E., Rizzi G.A., Tondello E. 1996. Pure and mixed phase Bi2O3 thin films obtained by metal organic chemical vapor deposition. Chem. Vap. Depos., 2(6), 238–242. doi: 10.1002/cvde.19960020605.
26. Condurache-Bota S., Tigau N., Constantinescu C. 2020. Effect of substrate temperature on bismuth oxide thin films grown by pulsed laser deposition. SN Appl. Sci., 2(3), 1–10. doi: 10.1007/s42452-020-2217-2.
27. Gadhi T.A., Gómez-Velázquez L.S., Bizarro M., Hernández-Gordillo A., Tagliaferro A., Rodil S.E. 2017. Evaluation of the photodiscoloration efficiency of β-Bi2O3 films deposited on different substrates by pneumatic spray pyrolysis. Thin Solid Films, 638, 119–126. doi: 10.1016/j.tsf.2017.07.037.
28. Sahoo A.K., Panigrahi M.R. 2022. Structural analysis, FTIR study and optical characteristics of graphene doped Bi2O3 thin film prepared by modified sol–gel technique. Results Chem., 4(October), 100614, 2022, doi: 10.1016/j.rechem.2022.100614.
29. Armelao L., Colombo P., Fabrizio M. 2002. Synthesis of Bi2O3 and Bi4(SiO4)3 Thin Films by the Sol-Gel Method. Entomol. Exp. Appl., 103(3), 239–248. doi: 10.1023/A.
30. Xiaohong W., Wei Q., Weidong H. 2007. Thin bismuth oxide films prepared through the sol-gel method as photocatalyst. J. Mol. Catal. A Chem., 261(2), 167–171, 2007. doi: 10.1016/j.molcata.2006.08.016.
31. Ilsatoham M.I., Alkian I., Azzahra G., Hidayanto E., Sutanto H. 2022. Effect of substrate temperature on the properties of Bi2O3 thin films grown by sol-gel spray coating. Results Eng., 17, 100991. doi: 10.1016/j.rineng.2023.100991.
32. Wang J. et al. 2023. One-step fabrication of Cu-doped Bi2MoO6 microflower for enhancing performance in photocatalytic nitrogen fixation. J. Colloid Interface Sci., 638, 427–438. doi: 10.1016/j.jcis.2023.02.005.
33. Ravele M.P., Oyewo O.A., Ramaila S., Mavuru L., Onwudiwe D.C. 2022. Facile synthesis of copper oxide nanoparticles and their applications in the photocatalytic degradation of acyclovir. Results Eng., 14(May), 100479. doi: 10.1016/j.rineng.2022.100479.
34. Morales-Mendoza J.E., Herrera-Pérez G., Fuentes-Cobas L., Hermida-Montero L.A., Pariona N., Paraguay-Delgado F. 2023. Synthesis, structural and optical properties of Cu doped ZnO and CuO–ZnO composite nanoparticles. Nano-Structures and Nano-Objects, 34, 100967. doi: 10.1016/j.nanoso.2023.100967.
35. Hemathangam S., Thanapathy G., Muthukumaran S. 2016. Optical, structural, FTIR and photoluminescence characterization of Cu and Al doped CdS thin films by chemical bath deposition method. J. Mater. Sci. Mater. Electron., 27(7), 6800–6808. doi: 10.1007/s10854-016-4630-2.
36. Ma Z., Ren F., Ming X., Long Y., Volinsky A.A. Cu-doped ZnO electronic structure and optical properties studied by first-principles calculations

and experiments. Materials (Basel)., 12(1), 2019. doi: 10.3390/ma12010196.

37. Mani Menaka S., Umadevi G., Manickam M. 2017. Effect of copper concentration on the physical properties of copper doped NiO thin films deposited by spray pyrolysis. Mater. Chem. Phys., 191, 181–187. doi: 10.1016/j.matchemphys.2017.01.048.
38. Manouchehri I., Mehrparvar D., Moradian R., Gholami K., Osati T. 2016. Investigation of structural and optical properties of copper doped NiO thin films deposited by RF magnetron reactive sputtering. Optik (Stuttg)., 127(19), 8124–8129. doi: 10.1016/j.ijleo.2016.06.005.
39. Nuaman R.T., Ali H.S. 2022. Study of the structural and optical properties of Bi2O3:Cu Thin FIlms as a Function of Different Doped Ratios. Math. Statictician Eng. Appl., 71(32), 1306–1315. doi: 10.1016/j.apsusc.2014.09.117.
40. Mane V.A., Dake D.V., Raskar N.D., Sonpir R.B., Stathatos E., Dole B.N. 2023. Magneto-optical properties of Fe-doped bismuth oxide nanorods for photocatalytic and antimicrobial applications. Results Chem., 6(August), 101083. doi: 10.1016/j.rechem.2023.101083.
41. Liu G., Lin Y., Li S., Shi C., Zhang D., Chen L. 2023. Degradation of ciprofloxacin by persulfate activated by Fe(III)-doped BiOCl composite photocatalyst. Environmental Science and Pollution Research, 30(37), 87830–87850. doi: 10.1007/s11356-023-28490-0.
42. Kaur A., Kansal S.K. 2016. Bi2WO6 nanocuboids: An efficient visible light active photocatalyst for the degradation of levofloxacin drug in aqueous phase. Chem. Eng. J., 302, 194–203. doi: 10.1016/j.cej.2016.05.010.
43. Alothman A.A. et al. 2023. Facile synthesis and comparative study of the enhanced photocatalytic degradation of two selected dyes by TiO2-g-C3N4 composite. Environ. Sci. Pollut. Res., 30(13), 37332–37343. doi: 10.1007/s11356-022-24839-z